www.sciencemag.org/content/363/6423/168/suppl/DC1

Supplementary Materials for

Emergence of preconfigured and plastic time-compressed sequences in early postnatal development

U. Farooq and G. Dragoi*

*Corresponding author. Email: george.dragoi@yale.edu

Published 11 January 2019, *Science* **363**, 168 (2019)
DOI: 10.1126/science.aav0502

This PDF file includes:

Materials and Methods

Subjects

Pregnant Long-Evans females (E9-E10) or litters with a dam (P4) were obtained from Charles River Laboratories and housed in a temperature-controlled room on a 12-hour light-dark cycle (light period: 7am-7pm) with ad libitum access to food and water. The pregnant female was checked 2-3 times a day and the day the litter was born was marked as P0 (postnatal day 0). The day of eye opening (P14) was used to confirm the age of animals. The pups were housed with the dam until P21. On P21, the pups were weaned, and littermates were housed together. Electrophysiological recordings were performed on 19 male rat pups aged P15-P24 on their day 1 of electrophysiological recording. For comparison purposes, the data obtained in the developing animals were grouped in two-day age groups of 3-5 animals starting at P15 (P15-16, P17-18, P19-20, P21-22, P23-24, see Supplementary Table 1 for number of animals/age group). Three adult male Long-Evans rats weighing ~350 g were used to compare the properties of neuronal ensembles in developing animals with those of adults.

Surgery and probe implantation

Surgery was performed under 1-2% isoflurane anesthesia administered intra-nasally. A heating blanket was used to maintain body temperature and regular checks were performed to ensure the depth of anesthesia. Two 32-site Neuronexus silicon probes (~20 microns between recording sites, 8 sites/shank, Buz32) attached to moveable microdrives were implanted bilaterally above each dorsal hippocampus around 3.0 mm posterior to bregma, 1.8 mm lateral to superior longitudinal sinus and 1.5 mm ventral to brain surface. One animal had a unilateral implantation of a moveable 64-site Neuronexus silicon probe (Buz64) at the same coordinates above the right hippocampus. The reference electrode (jeweler's screw) was implanted posterior to lambda in the cerebellum. The microdrives were secured to the skull with dental cement. Overall, the weight of the head mount was approximately 4 g and allowed unhampered free movement of the rat pups. After recovery from the surgery, the implanted developing rats were fed infant soymilk formula and were returned to the home cage for overnight housing with the mother and littermates. On the following three days after probe implantation, the probes were slowly lowered to the pyramidal layer of the CA1 subfield of the hippocampus while animals rested and slept in heated sleep boxes. The pups were separated from the mother for 2-4 hours on the days the probes were lowered toward the hippocampus and 4-6 hours on the days the experimental recordings were performed. The pyramidal layer was identified by the presence of prominent 140-250 Hz ripple oscillations, which were observed as early as P15, and by electrode depth. Once the probe location was optimized and stable recordings were obtained, the behavioral experiment was initiated. The adult rats were implanted bilaterally with either two moveable Neuronexus silicon probes (Buz64) or 32 moveable tetrodes as described earlier (*15*).

Behavior

The experiment was performed in one room. Hippocampal activity was recorded while the experimentally naïve rat pups slept in a heated high-walled opaque sleep box 20-20-30 cm for ~1.5 hour (Pre-Run sleep). Subsequently, the rats were placed on a 1-

meter-long novel linear track for the first time in their life, which they explored well without any prior training (*de novo* Run). Prior to the *de novo* Run session, rats were kept naive to linear tracks. The location of the sleep box was distinct from that of the linear tracks. Track running was followed by another sleep session in the sleep box (Post-Run sleep) recorded in the same location as the Pre-Run sleep. A subset of the rats from all group ages ran on the same linear track again on the same day (Day1Run2) before they were returned to their home cage. On day 2 of the experiment, all developing rats went through an additional and similar sleep-run on the same track-sleep protocol. All behavioral experiments were performed during the light phase of the day to maximize the probability of the animal sleeping. Animals were fed infant soy milk formula to supplement the diet they received from the dams. A similar sleep-run-sleep protocol was used for the adult animals, with longer sleep sessions (2-4 hours) and linear tracks (1.5 m long).

Electrophysiology

A 128-channel Neuralynx digital recording system (DigiLynx) was used to perform the recordings via a multiplexed lightweight cable connected to a head-mountable amplifier. Two LEDs (green and red) separated by 1.5 cm built into the headstage amplifier were used to continuously track the position of the animal, using an overhead camera. A counterbalanced sliding pulley system enabled free movement of the animals during the experiment. Wideband local field potentials (1-6000 Hz), >50 microvolts putative spike waveforms (600-6000 Hz), LEDs positions and a video of the experiment were simultaneously recorded using the DigiLynx system. Following the completion of the experiments, the animals were transcardially perfused with 0.9% saline followed by 4% paraformaldehyde, and the brains were harvested, sectioned and Nissl-stained with Cresyl violet to confirm the recordings were in the pyramidal layer of the dorsal hippocampal CA1.

Preprocessing and isolation of single units

Single units were isolated by a manual cluster-cutting procedure using Xclust3 software (*15, 25*) in a multidimensional space constituting the amplitude of detected spike waveforms on adjacent recording sites. Additionally, inter-spike intervals and cross-correlation measures were used to separate putative single units. Putative pyramidal units were distinguished from interneurons using autocorrelation, average firing rate and spike width. Only well-isolated units were used for further analysis. Animal position was extracted as the position of the two LEDs in the behavioral arena. Missing position samples were linearly interpolated.

Cluster quality and stability

Cluster quality was assessed by calculating the isolation distance of the clustered units from noise on their respective tetrodes (*31*). This procedure was followed separately for each session (Pre-Run sleep, Run and Post-Run sleep) to study cluster stability. A Pearson's product moment-correlation of age groups with cluster quality was computed to determine the relationship, if any, of cluster quality across age groups. To compare cluster quality across sessions in age groups, multiple comparisons with appropriate corrections for determining statistical significance were performed between each pair of

groups. Stability of clusters was also assessed by comparing the peak amplitude of the spike waveform for each cluster in the Pre-Run sleep and Post-Run sleep.

Place cell characterization

For each putative pyramidal unit, the number of spikes (when the speed of the animal exceeded 5 cm/s) in non-overlapping 1 cm bins were counted and smoothed by a 5 cm Gaussian kernel. This was divided by the occupancy (time spent at a speed above 5 cm/s, smoothed by a 5 cm Gaussian kernel) to determine the firing rate at each location. Pyramidal neurons with a peak firing rate exceeding 1 Hz were considered as place cells as described earlier (*15*).

Spatial information and within session stability

Spatial information (SI; bits/spike) quantifies the extent to which an individual place cell's firing is non-uniform across the spatial experience (conveying information about space). It was computed as follows (*18*):

$$SI = \sum_{j=1}^{L} Pr(loc_j) \frac{fr_j}{fr_{mean}} log_2(\frac{fr_j}{fr_{mean}})$$

where fr is the firing rate of the cell in location *j*, fr_{mean} is the mean firing rate of the cell, and $Pr(loc_j)$ is the probability of occupancy of location *j*. Within session stability of each place cell was computed by calculating Spearman's correlation of the place field maps derived from the first and the last quarter of laps during the Run session.

Bayesian decoding of spatial location during Run

Each direction of movement on the linear track was independently analyzed. To study the neuronal ensemble representation of space at the behavioral timescale, the activity of place-responsive pyramidal cells (with at least 10 spikes during Run) on the tracks was binned in 0.5 second non-overlapping bins during active behavior (animal velocity exceeding 10 cm/s). We employed a memoryless Bayesian decoding algorithm (*25, 32*). Briefly, according to Bayes' theorem,

$$Pr(loc|spk) = \frac{Pr(loc)\ Pr(spk|loc)}{Pr(spk)} = \frac{Pr(loc)\ Pr(spk|loc)}{\sum_{j=1}^{L} Pr(loc_j)\ Pr(spk|loc_j)}$$

where $Pr(loc|spk)$ is the posterior conditional probability of location given spikes, $Pr(loc)$ is the prior probability of location, $Pr(spk|loc)$ is the probability of spikes given a location, $Pr(spk)$ is the probability of spikes, loc_j is the j^{th} location on the track out of a total of L locations.

Assuming that spikes follow Poisson distributions and that place-responsive cells are statistically independent (*32*):

$$Pr(spk|loc) = \prod_{i=1}^{n} Pr(sp_i|loc) = \prod_{i=1}^{n} \frac{(\tau f_i(loc))^{sp_i}}{sp_i!} e^{-\tau f_i(loc)}$$

Therefore, inserting the above equation into Bayes' theorem, gives:

$$Pr(loc|spk) = Constant(\tau, spk)\, Pr(loc) \left(\prod_{i=1}^{n} f_i(loc)^{sp_i} \right) e^{-\tau \sum_{i=1}^{n} f_i(loc)}$$

where $Constant(\tau, spk)$ is a normalization factor such that $\sum_{i=1}^{Pn} Pr(loc_i|spk) = 1$, where $f_i(loc)$ is the value of the smoothed averaged place-responsive cell firing of the i^{th} place-responsive cell at location *l*, sp_i is the number of spikes fired by the i^{th} place-responsive cell in the time bin being decoded, τ is the duration of the time bin (0.5 seconds for active behavior on the track and 0.02 seconds for sleep frames) and *n* is the total number of place-responsive cells. $Pr(loc)$ is the prior for location, which was taken as uniform across the track.

For each bin, the location with maximum decoded probability was compared to the actual position of the animal and the error in the decoded position was determined. Time bins without any spikes were removed from this analysis. To study if the ensemble activity decoded the animal position above chance levels, the decoded posteriors across space were randomly permuted in time (500 time-bin shuffles) and the error in decoded position was recomputed and compared with that of non-shuffled data.

Error in decoding of animal location across the track during Run

To compare the decoding error across track locations during Run, we calculated the error within a moving window of 15 cm starting from the ends of the track. For this analysis, the track was folded at the middle, such that locations at equal distance from the track ends were averaged together. A Pearson's correlation between the distance from track ends and the median decoding error was computed.

Theta frequency

Theta frequency was calculated by isolating epochs with active behavior (velocity exceeding 10 cm/s) across all channels in the CA1, computing the Hilbert Transform and a Fast-Fourier Transform of the concatenated epochs of active behavior, and finding the peak frequency within the theta range (4-10 Hz). Additionally, to account for more subtle differences in animal velocities which could have been averaged out, we only used the theta cycles at animal velocities between 10-15 cm/s to compute the peak theta frequency for an age group in 10 channels per animal.

Theta sequences

Theta cycles during active behaviors (velocity exceeding 10 cm/s) were isolated. Cycles with a minimum of two neurons and occurring in the middle 2/5th of the track in the rat pups (30 cm from the ends of the track) were used for subsequent analyses. A window of 400 ms centered on the trough of each theta oscillation matching these criteria was extracted, and the Bayesian decoding of the population spike trains was performed to determine the virtual location of the animal based on the ensemble neural activity in 20 ms non-overlapping bins. For each theta cycle, this was centered on the current location of the animal (±30 cm) to reveal the difference between the actual and the predicted locations. Subsequently, the decoded relative locations were averaged across all theta cycles. A 100 ms window centered on the trough of the averaged theta cycle was used for computing the quadrant ratio. To study the modulation of theta sequences by the location of the animal, by the velocity of the animal, and by the number of cells per cycle, increasing thresholds for each of these parameters were set (velocity: 5 cm/s, 10 cm/s, 15 cm/s, 20 cm/s; location: a minimum distance of 20 cm, 30 cm and 40 cm from the ends of the track; minimum number of cells: 2, 3, 4). Animals with less than 30 theta cycles per threshold were not considered for this analysis.

Additionally, to accommodate for increasing theta frequencies with age, theta sequences were computed by binning the activity in theta phase (6 phase bins per theta cycle), instead of the 20 ms bin in the time domain, followed by Bayesian decoding of the ensemble neural activity. To accommodate for changes in theta power across ages, two analyses were performed. First, only the theta cycles within the top 25th percentile of the distribution of amplitude of theta cycles (peak-to-trough distance) were considered for theta sequence analysis. This tested whether theta sequences are absent at the younger ages even at the highest theta powers. Second, the theta cycles with the highest amplitude were dropped from the analysis at the older age groups (P17-18 onwards) and the theta cycles with the lowest amplitude were dropped from the P15-16 group until the average theta amplitudes of all age groups were equal or lower than the top 50th percentile of the theta amplitudes of the P15-16 group. Theta sequence analysis was performed on these restricted cycles to test whether increased theta power with age might account for the late emergence of theta sequences.

Quadrant ratio

The quadrant ratio quantifies the decoded theta sequential structure by adding the probabilities in the quadrants ahead (quadrant 1, future) and behind (quadrant 3, past) the current location of the animal in space and time and subtracting the other two quadrants from their sum. This difference is subsequently normalized by the sum of all probabilities in quadrants 1-4. Significance of theta sequences was determined by shuffling the time bins within theta cycles (n=500) and re-computing the quadrant ratio. If a group of animals had quadrant ratios significantly exceeding the 95th percentile of the shuffled distributions for that group, the group was considered to have significant theta sequences. Additionally, we calculated the proportion of individual significant animals, the latter defined as having an average quadrant ratio above the 95th percentile of the shuffled distributions and a spatial extent higher than 5 cm. To study the role of experience on theta sequences, an index (the quadrant ratio index) was computed. For each animal and

direction, the difference between the quadrant ratio of the data and the 95th percentile of the shuffled distributions was computed, and this difference was directly compared across the groups (experienced vs. non-experienced).

Properties of theta sequences

We calculated various properties of theta sequences to determine their representation of sequential spatial locations. First, we computed the best fit line of the averaged decoded theta sequence from neuronal tuning curves smoothed at 2 cm SD. This was determined by fitting all possible lines (in 1 cm steps) to the decoded posteriors and computing the ratio of sum of probabilities within 10 cm of the lines on one hand and the total sum of probabilities on the other. The fit with the maximal ratio was considered as the best fit (*25*). The encoding score was defined as the ratio for the best fit line and it quantifies the quality of encoding. To compute other properties of theta sequences, we considered all the lines with scores above the 95th percentile of the distribution of line fits, and for those fits the average slope/speed (cm/s), the spatial extent (in cm) and the compression ratio (average theta sequence slope divided by animal velocity) were computed.

Detection of frames during slow-wave sleep in the sleep box

Frames were detected during slow-wave sleep periods in the sleep box based on animal immobility (velocity below 2 cm/s, set at this value since the rat pups occasionally moved/twitched during sleep) and low theta/delta ratio on the LFP (epochs below the mean theta/delta ratio, computed on the Hilbert transform for the respective frequencies, 4-10 Hz for theta and 1-3 Hz for delta, and smoothed with a 10 s Gaussian) to exclude epochs of rapid-eye movement sleep. The non-REM sleep epochs were further reviewed manually and adjusted to ensure potential spurious detections of theta oscillation were excluded from further analysis. For the slow-wave sleep periods, the combined population activity of all pyramidal neurons in 1 ms bins was calculated and convolved with a Gaussian kernel of 15 ms. Periods when the population activity of at least 5 distinct place-responsive cells exceeded 2 standard deviations above the mean population activity for 100-800 ms during slow-wave sleep were considered as sleep frames for sequence analysis. Frames were binned at 20 ms. The number of spikes of each cell in each bin were counted and the Bayesian decoding of population spike trains was performed to determine the virtual position of the animal. Each direction was considered independent and analyzed separately for this analysis.

Detection of frames during on-track awake rest

Frames of activity were also detected during awake rest periods on the linear track. The criteria used for detection of frames during slow-wave sleep were applied during awake rest with the exception that animal velocity was kept at under 1 cm/s to prevent contamination from run behaviors.

Weighted correlations

To determine the sequential content within a frame, a product-moment linear correlation between time and location was computed, weighted by the associated posterior probabilities, $r(loc, t; Pr)$.

First the weighted mean was computed for location(m_{loc}) and time (m_t) as follows:

$$m_{loc}(loc;Pr) = \frac{\sum_{i=1}^{T}\sum_{j=1}^{L} Pr_{ij} loc_j}{\sum_{i=1}^{T}\sum_{j=1}^{L} Pr_{ij}}$$

Following computation of weighted mean for time in an equivalent manner, the next step involved computing the weighted covariance *(covar)*:

$$covar(loc,t;Pr) = \frac{\sum_{i=1}^{T}\sum_{j=1}^{L} Pr_{ij}(loc_j - m_{loc}(loc;Pr))(t_i - m_t(t;Pr))}{\sum_{i=1}^{T}\sum_{j=1}^{L} Pr_{ij}}$$

And, finally, the weighted correlation *(r)*:

$$r(loc,t;Pr) = \frac{covar(loc,t;Pr)}{\sqrt{covar(loc,loc;Pr)(covar(t,t;Pr))}}$$

where loc_j is the j^{th} spatial bin, t_i is the i^{th} temporal (20ms) bin in the frame, Pr_{ij} is the Bayesian posterior probability for the j^{th} spatial bin at the i^{th} temporal bin, T is the total number of temporal bins and L is the total number of spatial bins. Note that $\sum_{j=1}^{L} Pr_{ij} = 1$ and $\sum_{i=1}^{T}\sum_{j=1}^{L} Pr_{ij} = T$.

Probability score for stationary frames

The probability score for stationary frames was computed based on an iterative method adapted from previous reports (*15*, *25*) (see also Methods section on Properties of theta sequences). A line-fitting algorithm was used to detect the probability score of each frame. All possible lines (1 cm steps) were fit to the frame, and the ratio of sum of probabilities within 5 cm of the line on the one hand and the whole frame on the other hand was computed (probability score). The line maximizing this probability score was considered the best fit line for the frame and its associated score was used for comparison with shuffles.

Shuffles

To determine if individual frames significantly represented the experience, two types of shuffles were performed for each frame. First, the time bins within a frame were randomly permuted (time bin shuffle for theta sequences and trajectory sequences). Secondly, for detection of significant stationary frames, the decoded probability vector for each time bin of the frame was circularly shifted by a random amount between 1 and track length minus 1. This circular shift shuffle was performed for each bin independently

(space bin shuffle) as described earlier (*25*). This shuffle conserves the structure of decoded probabilities within a bin, but randomizes any association between bins.

Proportion of significant trajectory events

The proportions of significant trajectory sequences were calculated by comparing the weighted correlation of each individual frame with its respective shuffles (time-bin shuffle). Sequences/frames were considered significant if the weighted correlation exceeded the 97.5^{th} percentile or was below the 2.5^{th} percentile (for reverse sequences) of the shuffled distributions and the decoded spatial extent exceed 15% of track length. The proportion was calculated by dividing the number of significant frames by the total number of detected frames in that sleep session.

Proportion of significant individual animals with trajectory sequences

To study the emergence of preplay and replay at the individual animal level, frames for each direction were pooled, and the number of significant frames (assessed based on their respective shuffles) out of all frames were considered the 'successes' out of the total frames. A binomial test with $\alpha<0.05$ indicates significantly higher proportions of successes compared to chance.

Proportion of significant stationary frames

The significant stationary frames depicting individual locations were calculated by comparing the probability scores of the frames to their respective circular space-bin shuffles. If the probability scores for a frame were higher than the 95^{th} percentile of their shuffles and the spatial extent of decoded position was less than 5% of the track length, the activity within that frame was considered as significantly stationary and location-depicting. The proportion of significant stationary frames was calculated by dividing the number of significant stationary frames by the total number of detected frames in that sleep session.

Bias of awake stationary frames to current location

To determine if stationary frames during awake rest on the track were biased to initiate at the current animal location, the y-intercept of the fitted line was considered the starting location of the stationary frame. The differences in the actual position of the animal and the starting location were computed. In case of an initiation bias, the histogram of these differences should exhibit a peak at 0. To determine if this peak was significant, the probability of starting locations occurring within 20 cm of the current location of the animal was determined and was divided by the probability of starting locations occurring outside 20 cm of the current location. Subsequently, the histogram was shuffled (n=500), and this ratio re-determined. If the ratio in the data was higher than the 95^{th} percentile of the shuffled distribution, we concluded that there was a significant bias to the current location.

Ripple analysis

Ripple detection was performed by filtering the raw LFP in the 140-250 Hz range, during low theta-delta epochs and animal immobility (velocity less than 2 cm/s) in the sleep box. The mean ripple power in this band was computed, and periods exceeding 3

standard deviations of the mean were considered as hippocampal ripples and used for ripple characterization across development. To compute the ripple power within frames, the instantaneous ripple power was z-scored by the averaged ripple power. The maximal Z-scored ripple power in the frame was considered as its associated ripple power.

Compression ratio

Time-compression of decoded trajectory sequences relative to their behavioral timescale activation was computed by calculating the ratio between the speed of the decoded trajectory sequence during sleep/rest/run and the average speed of the animal during the Run session.

Sequence score

The sequence score (r_Z) was defined as the Z-score of the absolute weighted correlation of a frame relative to the distribution of absolute weighted correlations of its shuffled frames (*28*). It was computed as follows:

$$r_Z = \frac{|r| - mean(|r(shuffles)|)}{std(|r(shuffles)|)}$$

where r is the weighted correlation of the frame and $r(shuffles)$ the weighted correlations of its respective shuffles.

Plasticity at the individual animal level

Sequence scores for frames in both directions were pooled for each animal in the Pre-Run sleep and Post-Run sleep, subsequently the sequence scores for the sleeps were compared using a ranksum test.

Jump distance

During the frames, the peak decoded virtual position along the animal's trajectory was computed for each time bin. The median of the absolute differences between peak decoded locations in consecutive bins divided by the length of the track was considered the median jump distance of that frame, while the maximum of jumps was considered the maximum jump distance. To account for the effect of frame length on its value, the maximum jump distance was subsequently normalized by the maximum jump distances of its respective time-bin shuffles (expressed as a percentile of the shuffled distribution, i.e., normalized maximum jump distance).

Proportion of significant frames using two additional criteria for significance

To determine if frames could simultaneously pass additional two criteria (i.e., in addition to the time-bin shuffle), thresholds for weighted correlation and maximum jump distance were set, and only frames matching these criteria were compared to their respective shuffles. In this regard, only the frames with the top 70th percentiles of frames as assessed by weighted correlations and bottom 70th percentiles of maximum jump distances were analyzed, and their weighted correlation compared to shuffles as described before. A percentile was used rather than a fixed threshold since the weighted correlation was observed to be correlated to the extent of the frames. These criteria effectively used

only the best ~50% of the data for further quantification. These criteria were empirically set based on significance in frames from adult animals.

Simultaneous two-feature comparison of absolute weighted correlations and maximum jump distances between frames and shuffles

We additionally simultaneously quantified and compared the weighted correlations and maximum jump distances of frames in a session (slow-wave sleep or awake rest) with that of their respective time-bin shuffles (n=500). The data and the corresponding shuffles had the same frame lengths. All detected frames in the sleep were used for this analysis. To simultaneously study weighted correlations and maximum jump distance of frames, increasing thresholds for weighted correlations and decreasing thresholds for jump distance were independently applied to a particular sleep session, and the proportion of frames passing both thresholds were calculated (*33*). The values of the thresholds for these features were: 0 to 0.9 in steps of 0.1 for weighted correlation, and 0.1 to 1 in steps of 0.1 between successive thresholds for maximum jump distance. The number of all shuffles with proportion of frames less than the data passing those thresholds were counted and divided by the total number of shuffles (n=500). This value was subsequently subtracted from 1 to be expressed as a P-value, with significance set at $P<0.05$. The P-values were plotted as a pseudo-colored significance matrix.

Simultaneous two-feature comparison of sequence scores and median jump distances/normalized maximum jump distances between Pre-Run sleep and Post-Run sleep frames

Single features of trajectory sequences do not completely describe their properties. Therefore, we simultaneously compared the two most sensitive features between Pre-Run sleep and Post-Run sleep frames, sequence score and jump distance, to reveal any potential differences not observed in our analysis on the proportion of significant frames. All detected frames in the sleep were used for this analysis. Because Pre-Run and Post-Run sleep frames of different lengths had differing sequential content, we computed the jump distance using the median jump distance value, which does not depend on the frame length. We obtained similar results using the normalized jump distance value, which also does not depend on the length of the frame. To simultaneously study sequence score and median jump distance of frames, increasing thresholds for sequence score and decreasing thresholds for jump distance were independently applied to a particular sleep session, and the proportion of frames passing both thresholds were calculated. The values of the thresholds for these features were: no threshold (i.e., all frames), 0 to 2.8 in steps of 0.4 for sequence score, and 0.125 to 1 in steps of 0.125 between successive thresholds for median jump distance. A one-tailed Z-test of two proportions (Post-Run sleep>Pre-Run sleep) was performed for each set of thresholds (72 sets in total) between the Post-Run sleep and the Pre-Run sleep proportion of frames exceeding the respective thresholds. The resultant Z-score for each set of thresholds was expressed as a P-value, with significance set at $P<0.05$. The P-values were plotted as a pseudo-colored matrix. Additionally, to ensure sequences without large maximum jumps were plastic, we simultaneously compared the sequence scores and normalized maximum jump distances between Pre-Run and Post-Run sleep, using a similar statistical method. The maximum jump distance was normalized (by computing a percentile of it relative to its frame-

matched time-bin shuffles) for comparison across sleeps because a relationship between frame length and maximum jump distances was observed in our data.

Equalizing decoding errors on and across track

To account for the age-dependent decrease in decoding errors during the Run on observing sequential structure in the sleep, we removed the neurons with the highest spatial information in the P23-24 group until its median decoding error and distribution of decoding errors across the track matched that of the P15-16 group. Subsequently, we performed the same sleep analysis on this error-matched dataset.

Controlling for differences in experience within a Run session

Laps were considered as runs across the track (at velocities exceeding 10 cm/s) covering a minimum of 0.7 of the track length. Although we did not observe a correlation of number of laps run by the freely behaving animals and/or lap incidence with age, we nonetheless controlled for these factors by two methods. First, we used only the first 17 laps during the Run (i.e., the observed average number of laps in the group with the least number of laps) for quantification and analysis of theta sequences and sleep sequences for groups with higher number of laps (P15-16, P21-22 and P23-24) and all laps in the remaining groups (P17-18 and P19-20). To further control for the role of experience during Run on sequence plasticity, we only studied plasticity in the subset of animals with similar lap properties (i.e. P15-16: 3 animals, P21-22: 2 animals and P23-24: 2 animals for number of laps and P15-16: 3 animals, P17-18: 3 animals, P21-22: 1 animal, P23-24: 2 animals for lap incidence) at the individual animal level.

Generation of Poisson surrogate datasets

To determine if differences in firing rates across cells could account for the observation of trajectory sequences and stationary frames at various ages, the mean firing rate of each neuron within all frames in Pre-Run sleep was computed. Subsequently, surrogate datasets (500 datasets) were generated with each corresponding cell exhibiting the same mean firing rate, but otherwise random firing characteristics (according to a homogenous Poisson process). The absolute weighted correlations of each iteration of these surrogate datasets were compared to the real data using a Wilcoxon's ranksum test. Furthermore, we shuffled one surrogate dataset and determined if significant trajectory sequences and stationary frames could be detected, using the same methods/shuffle procedures as those used for trajectory sequences and stationary frames in the real data. Additionally, a two-feature comparison of the Poisson was performed as in the real data (described in the earlier sections) to determine if any spurious trajectory sequences were detected due to firing rate inhomogeneity across hippocampal neurons.

Statistical tests

To determine the relationship of age to various ensemble properties, a product-moment linear Pearson's correlation or an omnibus test (one-way analysis of variance; ANOVA) was performed followed by posthoc Tukey's tests for multiple comparisons. Parametric statistical tests (one-sample and two-sample Student's t-tests) were performed on data that did not violate the normality assumption. Otherwise, non-parametric statistical tests (Kruskal-Wallis ANOVA followed by posthoc Dunn's tests, Wilcoxon's

ranksum test or the Wilcoxon signed rank test) were performed. A $P<0.05$ was considered significant. ***$P<0.001$, **$P<0.01$, *$P<0.05$, ns=not significant. P-values smaller than 10^{-10}, were presented as $P<10^{-10}$.

Examples in figures

For plotting purposes only, a smoothing of 2cm SD was applied to the raw tuning curves in Figure 1H, a moving window (20 ms advanced in steps of 5 ms) was used for displaying theta sequences in Fig. 2. Similarly, a moving window (20 ms advanced in steps of 10 ms) was used for displaying sequences in awake rest and sleep (Figs. 3, 4, S8). Frame durations provided with the frames were rounded up to the nearest 20 ms.

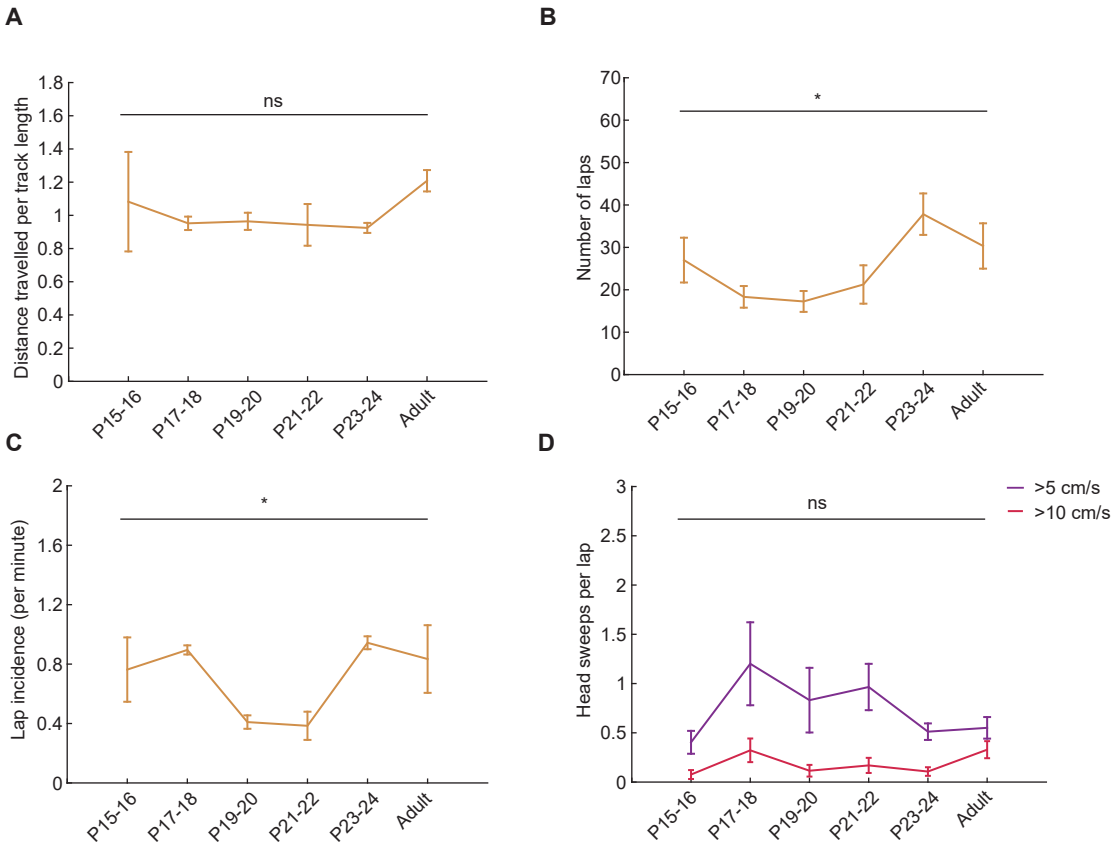

Fig. S1. Across-development micro-features of animal behavior during Run on the track. (**A**) Total distance travelled per track length in a lap is unaffected by age (P>0.05, ANOVA). (**B**-**C**) Average number (**B**) and incidence (**C**) of laps scored during de novo Run session exhibit a U-shaped relationship with age (P<0.05, ANOVAs). Although some variability was observed across groups, the number of laps (R=0.22; P=0.15) and incidence (R=0.02; P=0.91) did not exhibit significant correlations with age. (**D**) Head sweeps at two velocity thresholds during running do not change with age (P>0.05, ANOVAs). *P<0.05, ns=not significant.

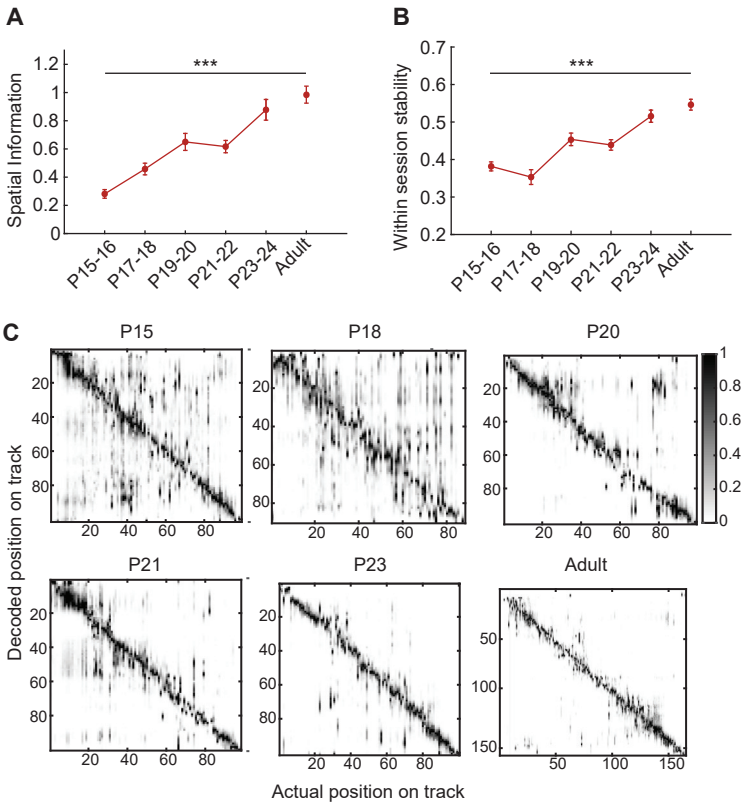

Fig. S2. Development of CA1 place cell and neuronal ensemble representations of space during first-time navigation on a linear track. (**A**) Spatial information of putative CA1 place cells (peak rate >1Hz) increases with age across development ($P<10^{-10}$, ANOVA). (**B**) Within-session stability of place fields increases across development ($P<10^{-10}$, ANOVA). (**C**) Confusion matrices depicting actual and decoded animal position during first-time navigation across development. Note that ensemble activity can reliably represent the location of the animal during Run as early as P15. Data are means ± SEM. ***$P<10^{-10}$.

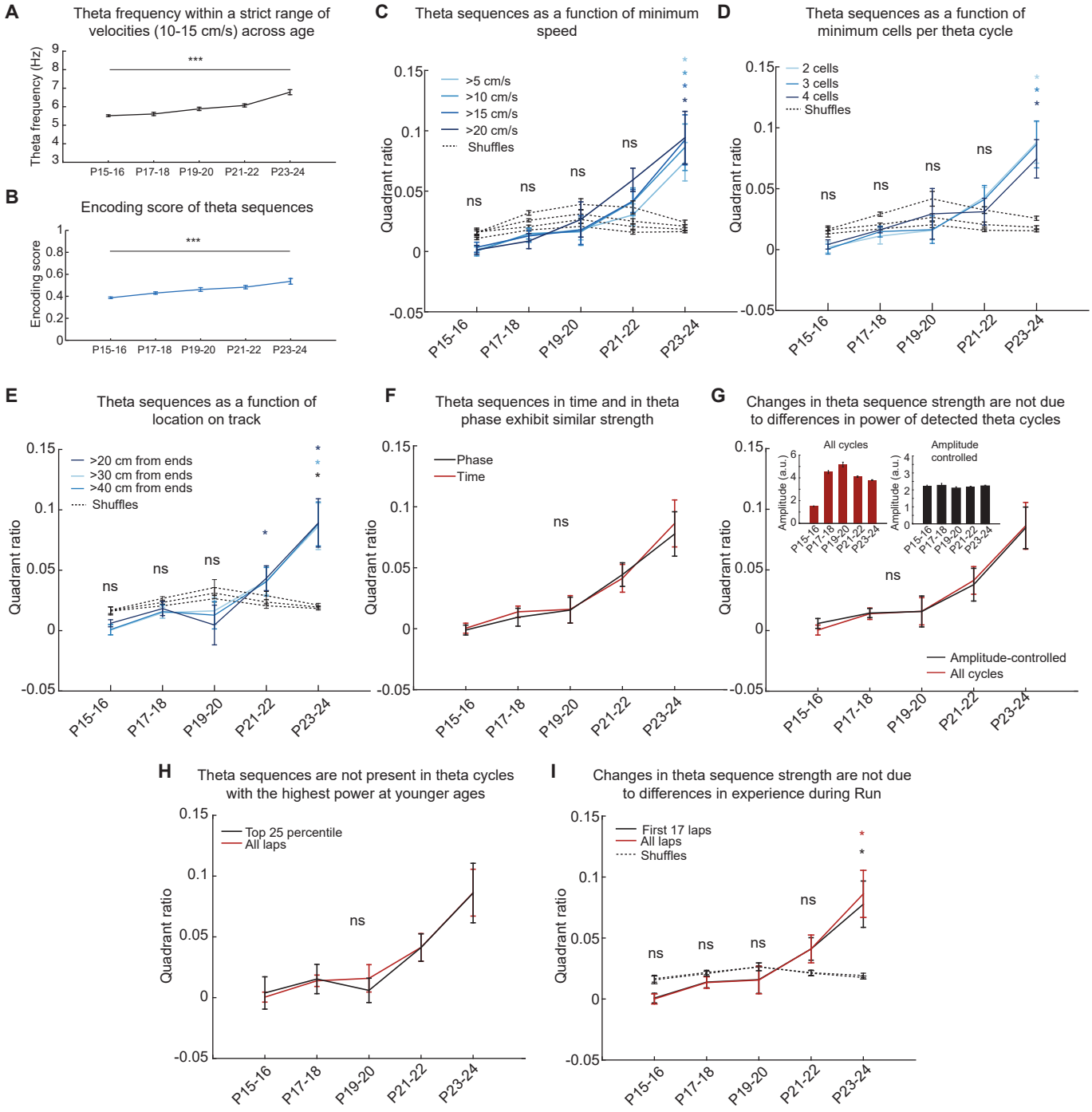

Fig. S3. Reliability of theta sequence analysis using Bayesian decoding. (**A**) Theta frequencies computed within a narrow range of velocity (>10 cm/s and <15 cm/s) increase with age (ANOVA, $P<10^{-10}$). (**B**) Encoding score of theta seqeunces increases with age (ANOVA, $P<10^{-10}$). (**C**-**F**) Strength of theta sequences is not significantly affected by: the speed of the animal (**C**), changes in the minimum number of cells per theta cycle (**D**), the location of the animal on the track (**E**) and computation in the phase or in the time domain (**F**, P<0.05, paired t-tests). Only the P23-24 group had significantly higher quadrant ratio compared to shuffled datasets at any and all: speed thresholds (P<0.05, paired t-tests), cell number thresholds (P<0.05, paired t-tests), on-track location (P<0.05, paired t-tests). P21-22 group was significantly higher than shuffles for the on-track location threshold >20 cm from ends (P<0.05, paired t-test). (**G**-**H**) Changes in theta sequence strength across development are not due to changes in the amplitude of theta oscillation power. Quadrant ratios computed from all theta cycles are similar to the ones computed from theta amplitude matched cycles (**G**) or from the top 25th percentile of the distribution of theta cycle amplitudes (**H**) across all age groups during development. Changes in theta oscillation amplitude appear to assume an inverted U-curve across development (**G**, left inset) and subsampling only similar amplitudes of theta cycles (**G**, right inset) revealed similar results. (**I**) Theta sequence quadrant ratio computed from only the first 17 Run laps (smallest mean number of laps for an age group) shows similar values to when all Run laps are considered. Data are means ± SEM. ***$P<10^{-6}$, *P<0.05, ns=not significantly higher.

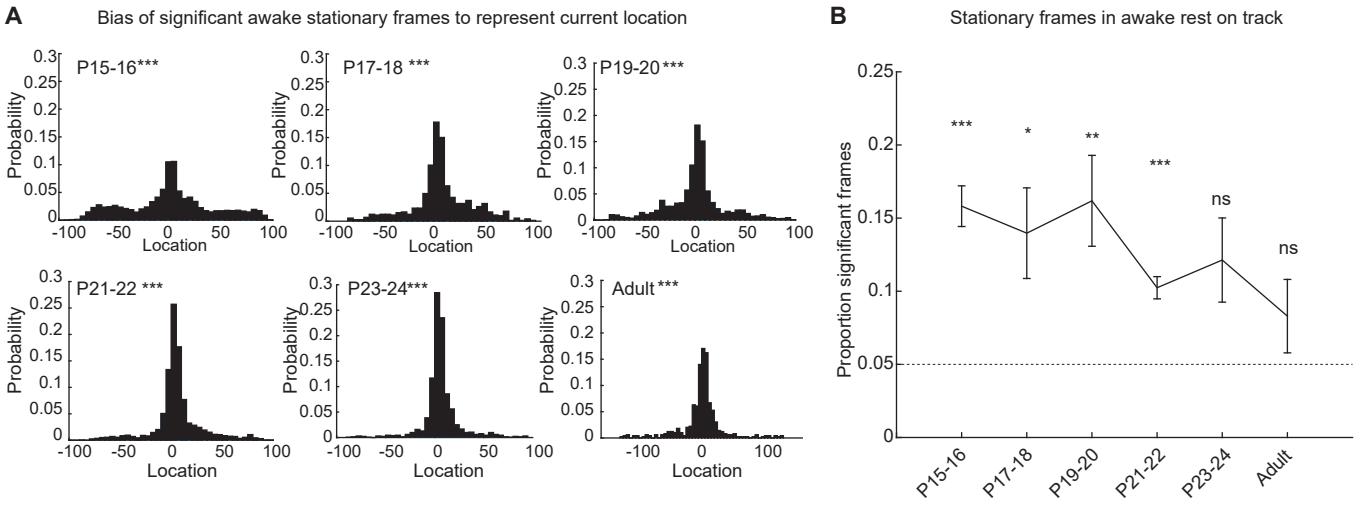

Fig. S4. Stationary frames during awake rest on the track. (**A**) Stationary frames are biased to represent the current location of the animal, as early as P15-16. P-values are computed by comparison to shuffles. (**B**) Proportion of stationary, individual location-depicting frames approaches chance levels at P23-24 (t-tests against chance). ns=not significant. ***P<0.005, **P<0.01, *P<0.05, ns=not significant.

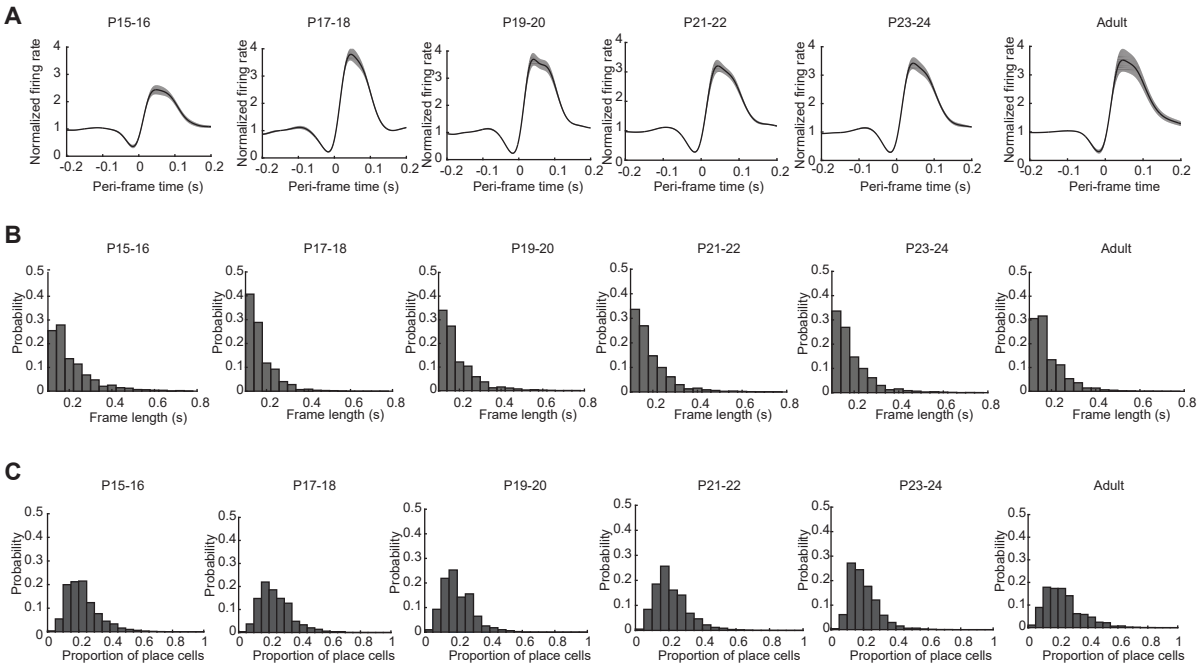

Fig. S5. Neuronal ensemble activity during sleep frames has similar temporal dynamics across development. (**A**) Increased multiunit ensemble activity at the beginning of frames (time 0) can be observed throughout development. (**B**) Mild variability in frame length with age across development ($P<10^{-3}$, Kruskal-Wallis ANOVA; however, posthoc comparisons to adult: all groups $P>0.05$, Dunn's tests). (**C**) Proportion of place cells active within frames is similar across development ($P>0.05$, Kruskal-Wallis ANOVA).

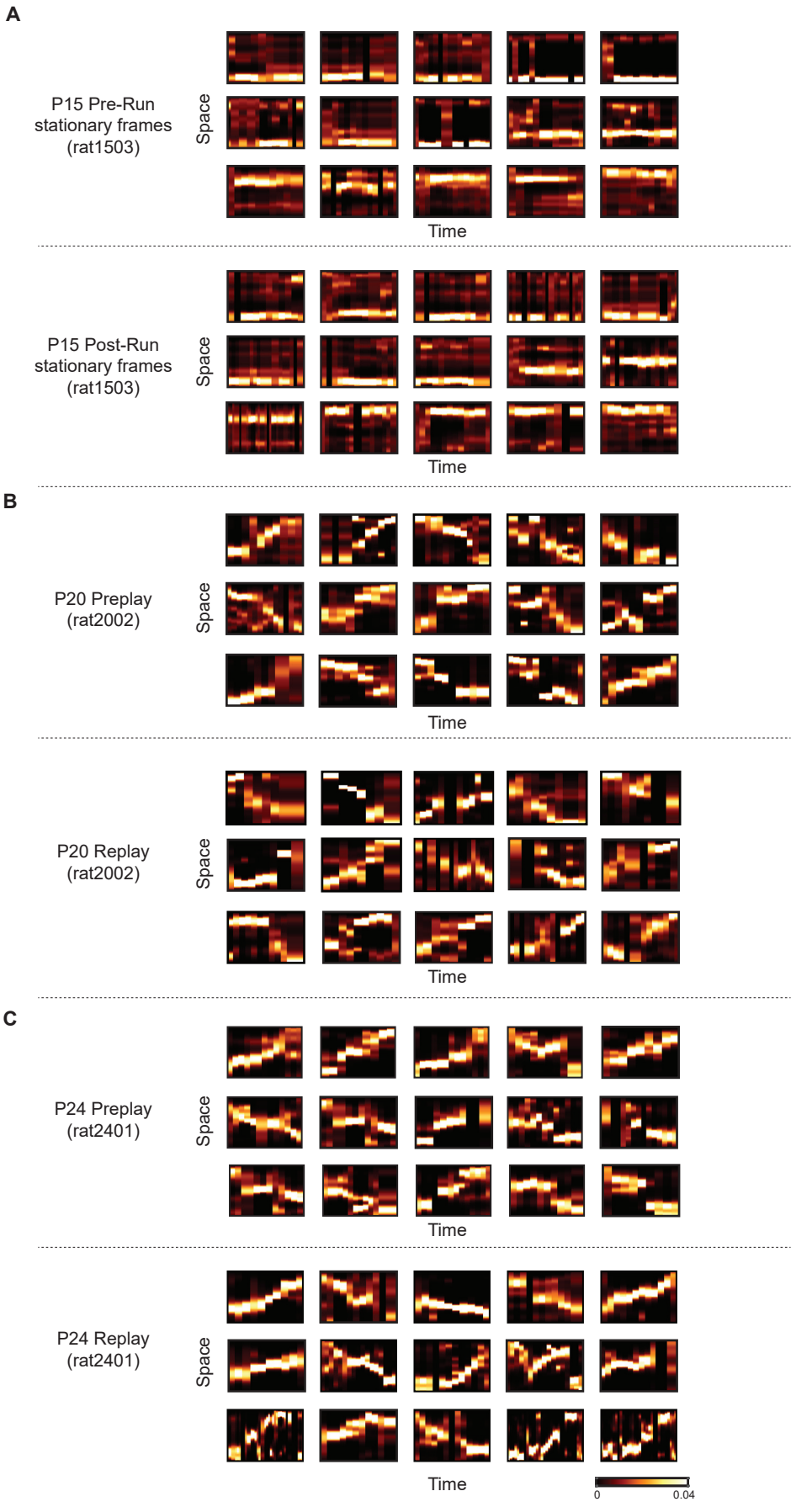

Fig. S6. Examples of decoded stationary frames and trajectories at different ages. (**A-C**) Stationary frames at P15 (rat1503) and trajectory sequences at P20 (rat2002) and P24 (rat2401) in the sleep before and after exposure to a linear track for the first time.

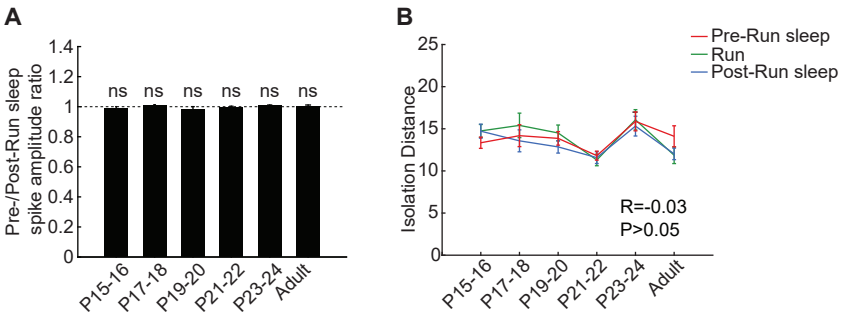

Fig. S7. Similar cluster quality across different age groups. (**A**) Ratio of average spike amplitude in Pre-Run sleep to Post-Run sleep is not different across age groups (ANOVA, P>0.05) and approaches unity in each age group (t-tests, P>0.05). (**B**) Isolation distance value for the recorded neurons does not increase with age or between sessions [Pearson's correlation, age vs. isolation distance (all sessions): R=-0.03, P=0.12; (Pre-Run sleep) R=0.03, P=0.36; (Run) R=-0.05, P=0.06; (Post-Run sleep) R=-0.05; P=0.10]. Cluster quality was uncorrelated with the emergence of theta sequences (R=-0.0045, P=0.88), preplay (R=0.019, P=0.53) and plasticity (R=0.0084, P=0.78). Data are means ± SEM. ns=not significant.

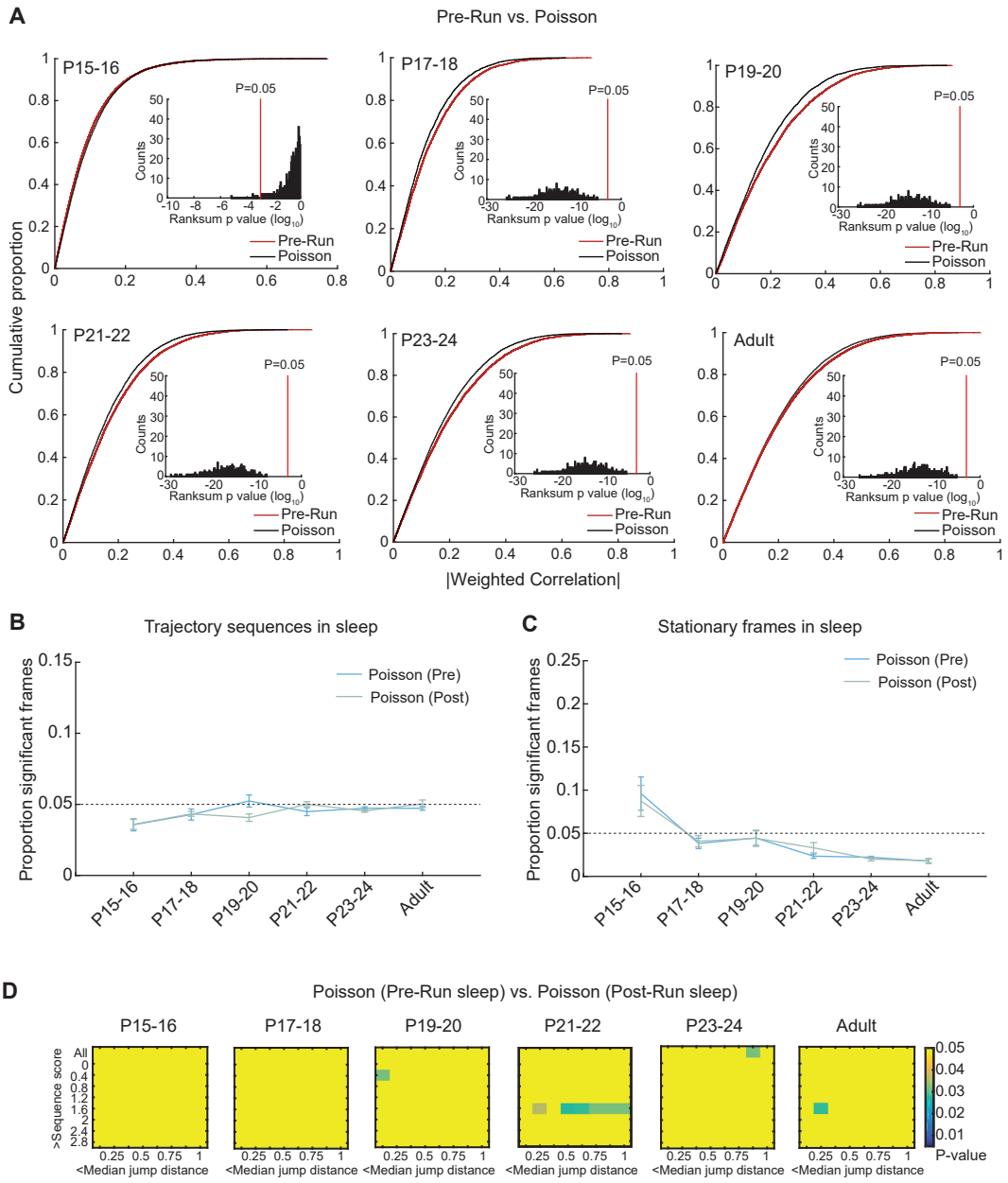

Fig. S8. Neuronal ensemble temporal organization observed in sleep exceeds that of surrogate stochastic datasets with conserved neuronal firing rates. (**A**) Pre-Run sleep frames in P17-18 and older animals have significantly higher weighted correlations compared to their respective Poisson-distribution surrogate datasets (500 iterations; 500/500 iterations were significantly higher as depicted by the ranksum P-values in the insets; $P<10^{-10}$, binomial test for significant iterations). In contrast, at P15-16, the Poisson distributions had significantly higher structure than the Pre-Run sleep data in 7/500 iterations ($P<0.05$, binomial test for Pre-Run sleep>Poisson). This indicates that neuronal sequential structure exceeds the one resulting from neuronal firing rate dynamics starting at P17-18 (cumulative proportions for one example surrogate Poisson dataset and the Pre-Run sleep dataset are plotted). (**B**) Poisson surrogates lack significant sequential structure above chance levels at all tested age groups. Proportion of significant frames were either at or below chance levels, Pre-Run/Post-Run sleep: P15-16, P=0.008/0.003; P17-18, P=0.127/0.010; P19-20, P=0.595/0.009; P21-22, P=0.107/0.962; P23-24, P=0.041/0.004; adult, P=0.089/0.902, t-tests. (**C**) Proportions of Poisson-surrogate stationary frames are at or below chance beginning at P17-18 (Pre-Run/Post-Run sleep: P15-16, P=0.041/0.067; P17-18, P=0.112/0.220; P19-20, P=0.534/0.553; P21-22, P<0.001/0.027; P23-24, P<0.001/0.001; adult, P<0.001/0.001, t-tests) and below proportion of stationary frames during Pre-Run sleep at P15-16 (P=0.001/0.001, t-tests). (**D**) Two-feature comparison of firing-rate matched Poisson surrogate datasets for Pre- and Post-Run sleep show no difference at any age, demonstrating the observed plasticity is not due to changes in firing rates. Data are means ± SEM.

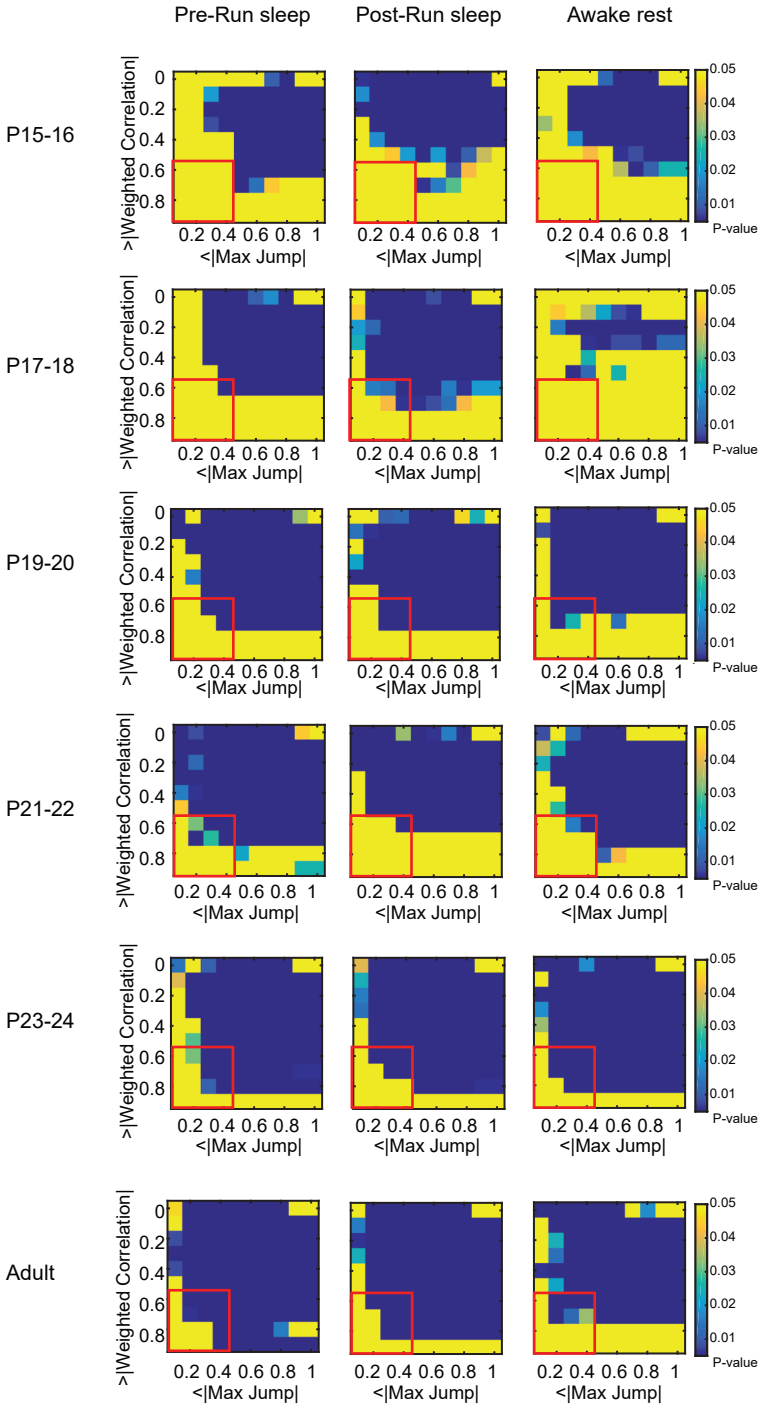

Fig. S9. Two-feature comparison of trajectory sequences to their shuffles across development. Simultaneous weighted correlation and maximum jump distance comparison between Pre-Run sleep, Post-Run sleep, Awake rest frames with their respective time-bin shuffles. Note this analysis reveals that the real data has more structure than the shuffles, not that significant trajectory sequences occur above chance levels (as in Figure 4B). Red squares indicate thresholds with high weighted correlations and low maximum jump distances (as in Ref. *33*), which are met first in Pre-Run sleep at P17-18.

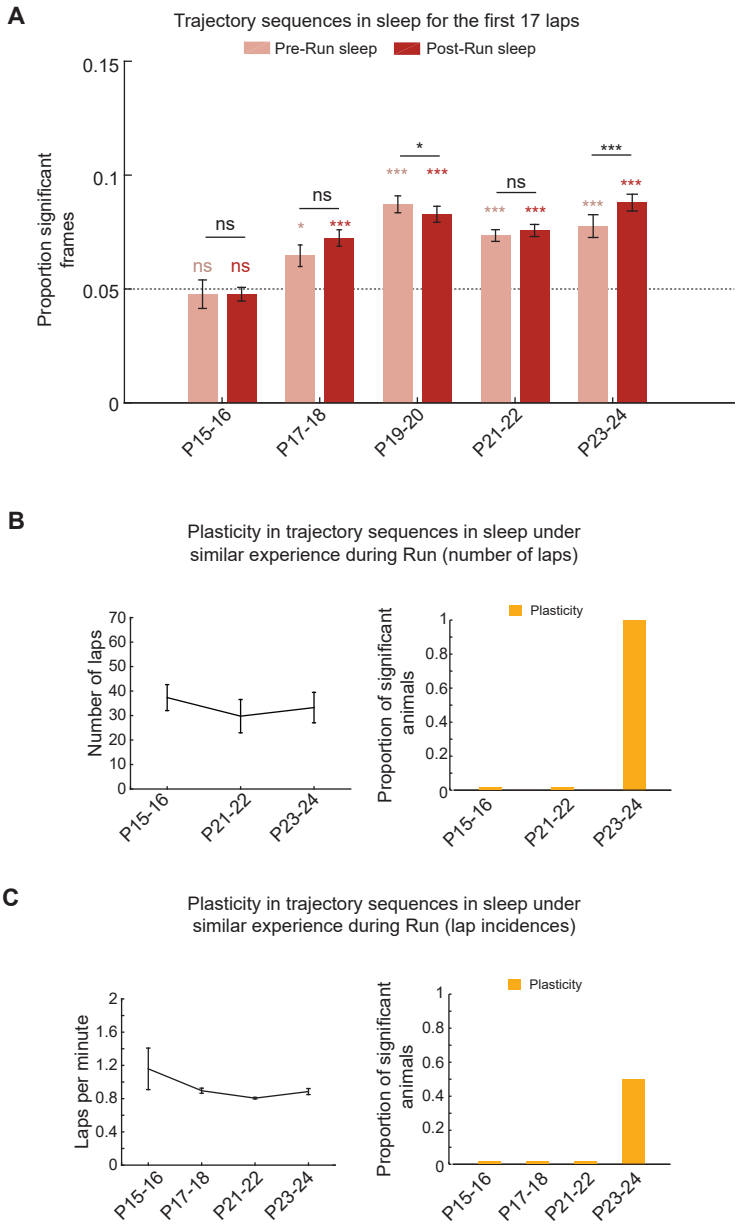

Fig. S10. Controlling for changes in micro-features of behavior on the track across development. (**A**) Proportions of trajectory sequences in sleep when only the first 17 Run laps for each animal were used for computation of spatial tuning curves (for animals belonging to groups with higher average number of laps). Note similar results compared to Fig. 4B when all Run laps were analyzed. (**B**) Right panel: Proportion of significant individual animals in sleep when only animals with similar number of laps from each group matching the P23-24 group (n=3, 2, 2 animals/group). Left panel shows the average number of laps in the animals analyzed. (**C**) Right panel: Proportion of significant individual animals in sleep when only animals with similar Run lap incidence were separately analyzed (n=3, 3, 1, 2 animals/group). Left panel shows the average lap incidence in the animals analyzed. Note all animals between P15-P22 showed no plasticity at the individual animal level (Fig. 4B) regardless of the experience during the first Run session. Data are means ± SEM. ***P<0.005, *P<0.01, *P<0.05, ns=not significant.

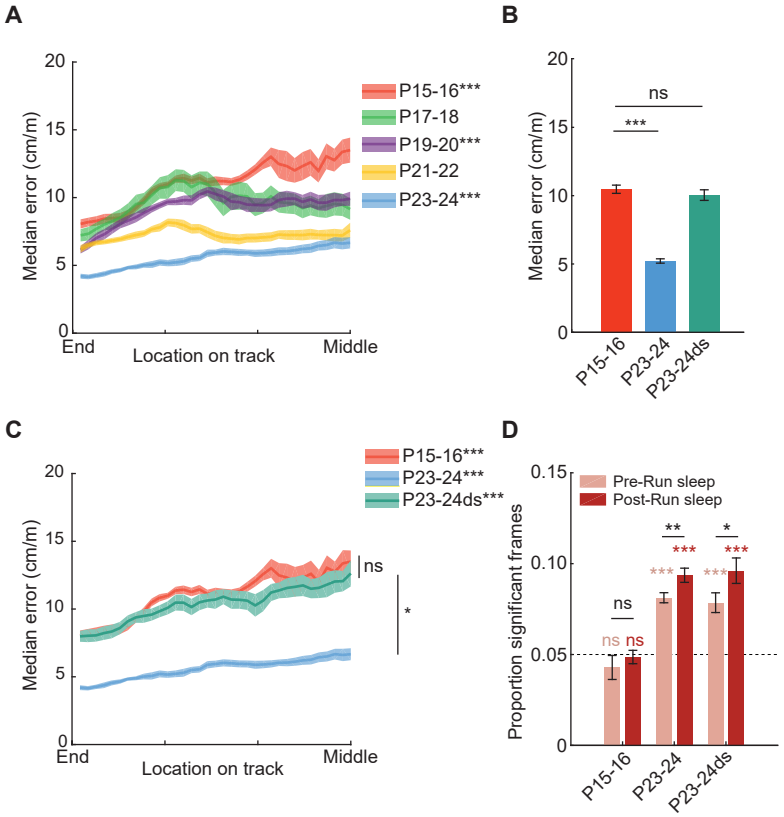

Fig. S11. Higher decoding error in the middle of the track does not account for lack of preplay and replay at P15-16. (**A**) Decoding error during Run is higher in the middle of the track in the P15-16, P19-20 and P23-24 groups and uniform for the remaining age groups as assessed via correlation between distance from boundary and median decoding error. (**B**-**C**) Decoding analysis performed after removing top 50% of the cells with the highest spatial information in P23-24 animals. This procedure increased the decoding error of P23-24 animals to the level of P15-16 animals (**B**) and resulted in datasets (i.e., P23-24ds) having a similar distribution of decoded errors across the track as the P15-16 animals (**C**). Multiple-way ANOVA: age (P15-16 vs. P23-24ds), $P>0.05$; location on track $P<10^{-10}$; interaction between age vs. location $P>0.05$. (**D**) Proportion of significant trajectory frames in sleep across the three groups. Note that, despite controlling for these two factors (i.e., median decoding error on track and distribution of decoding errors across the track), we observed preplay, replay and plasticity during sleep in P23-24ds animals. This indicates that increased decoding error alone could not account for the lack of preplay and replay at P15-16. Data are medians ± SE (**A**-**C**) and means ± SEM (**D**). ***$P<10^{-10}$, **$P<0.01$, *$P<0.05$, ns=not significant.

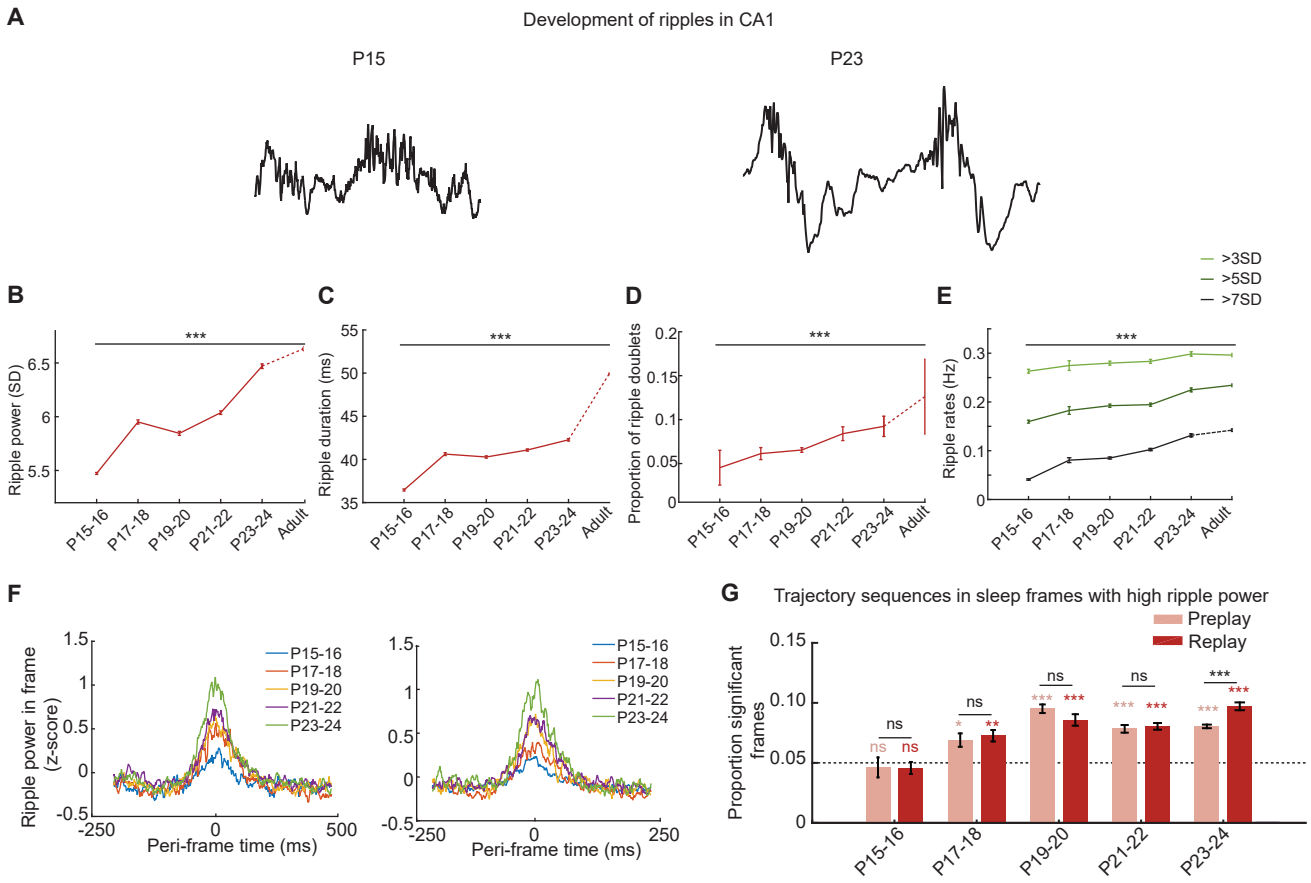

Fig. S12. Development of ripple (140-250 Hz) activity and of ripple-associated trajectory-depicting sequential activity. (**A**) Examples of ripples at P15 and at P23. (**B**-**E**) Age-related increases in ripple: mean power (**B**; in standard deviations above mean), duration (**C**), proportion of doublets (**D**; within 200 ms), and incidence at various thresholds (**E**). $P<10^{-10}$, ANOVAs (**B**-**E**). (**F**) Increase in median ripple power coinciding with an increase in multiunit activity in frames with significant trajectory-depicting sequences (left panel) and significant location-depicting ensembles (right panel). (**G**) Sleep frames with high ripple power (>3 standard deviations above mean) exhibit similar proportions of significant proportions of trajectory sequences compared with those of all sleep frames (see Fig. 4B; paired t-tests). ***P<0.005, **P<0.01, *P<0.05, ns=not significant.

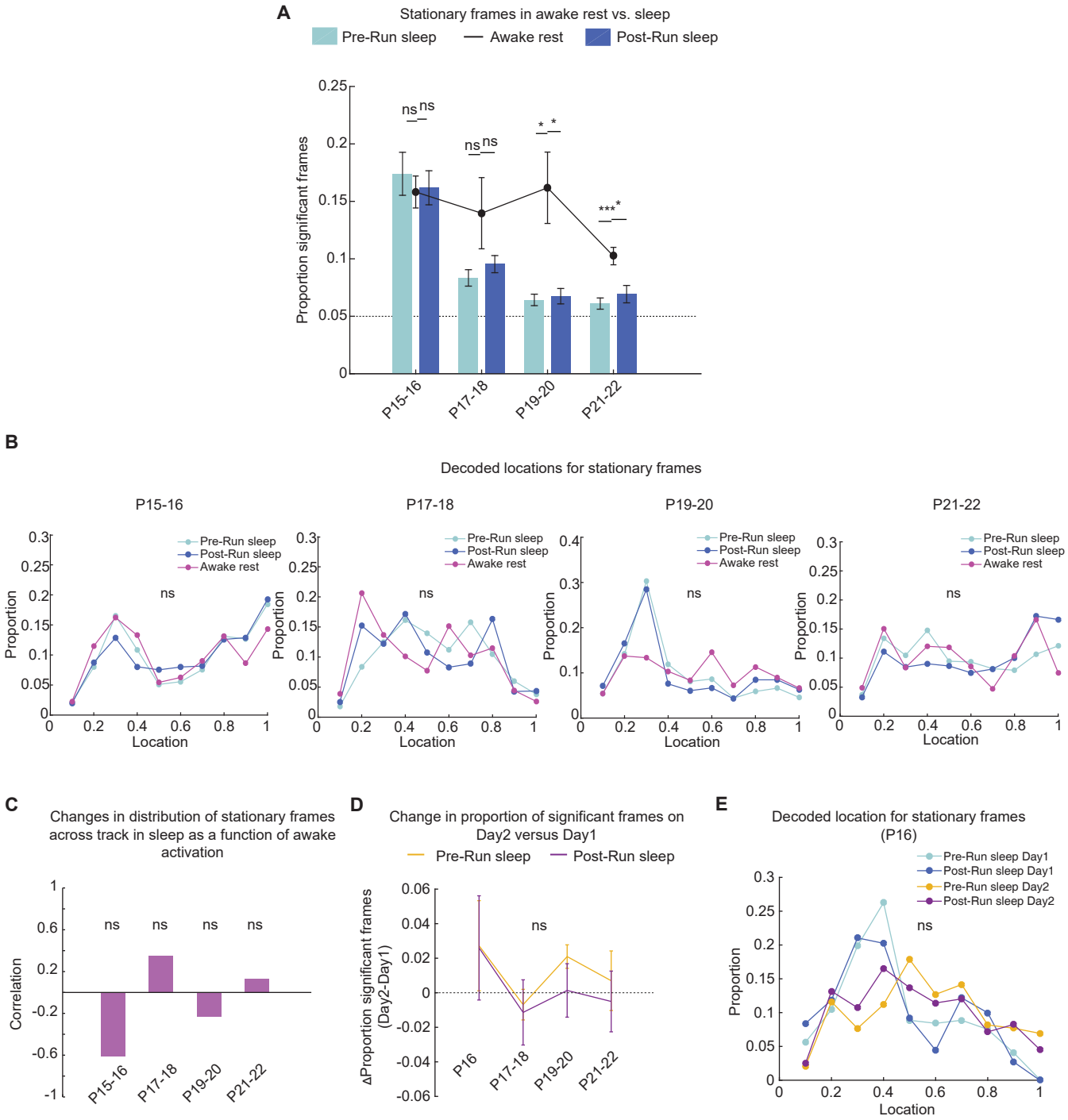

Fig. S13. Stationary frames during awake rest and sleep on the track. (**A**) Proportion of stationary, individual location-depicting frames is transiently higher during awake rest compared to sleep early in development (P19-22). (**B**) Distribution of on-track locations decoded from stationary frames in Pre-Run sleep, Awake rest and Post-Run sleep across age groups with significant proportions of stationary frames are similarly distributed across the track (Kolmogorov-Smirnov tests between all pairs of brain states, P>0.05; in addition, we tested individual animals separately and found no significant differences in any animal at any age). (**C**) Correlation of changes in proportion from Pre-Run to Post-Run sleep with proportion across track during awake rest. No group at any age showed a significant correlation. (**D**) Change in the proportions of stationary frames recorded on Day 1 vs. Day 2 during Pre- and Post-Run sleep in age matched animals (n=3, 3, 1, 3/group; 2 directions per animal). Note changes are not influenced by the Run experience and the previous day experience (all t-tests in P15-16, P17-18 and P21-22 groups, P>0.05). (**E**) Distribution of on-track locations decoded from stationary frames in Pre-Run sleep and Post-Run sleep during first-time Run (Day1Run) and Day2Run at P16 (Kolmogorov-Smirnov tests between all pairs, P>0.05). ***P<0.005, **P<0.01, *P<0.05, ns=not significant.

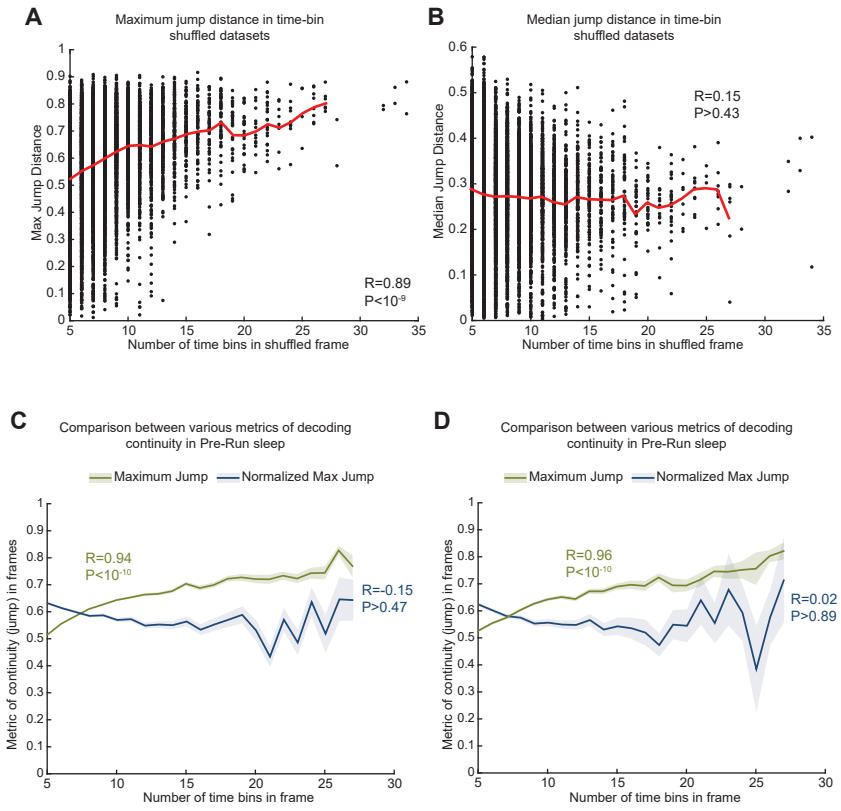

Fig. S14. Maximum jump distance is a biased estimator for experience-dependent plasticity. (**A**) The maximum jump distance in shuffled datasets increases with frame length. The maximum jump distance is biased towards detecting significance in shorter frames. (**B**) The median jump distance was unaffected by the frame length. (**C**-**D**) The maximum jump distance in the real frames increased with the number of time bins in the frame, while the normalized maximum jump distance did not increase with the number of time bins in the frame in the Pre-Run sleep (**C**) and Post-Run sleep (**D**). Based on the observed relationship between max jump distance and frame length (**A**), we subsequently normalized the jump distance of a frame relative to its shuffles before comparing it between Pre- and Post-Run sleep. These quantifications were performed on data from the adult rats group. For (**A**-**B**) red line indicates the running mean.

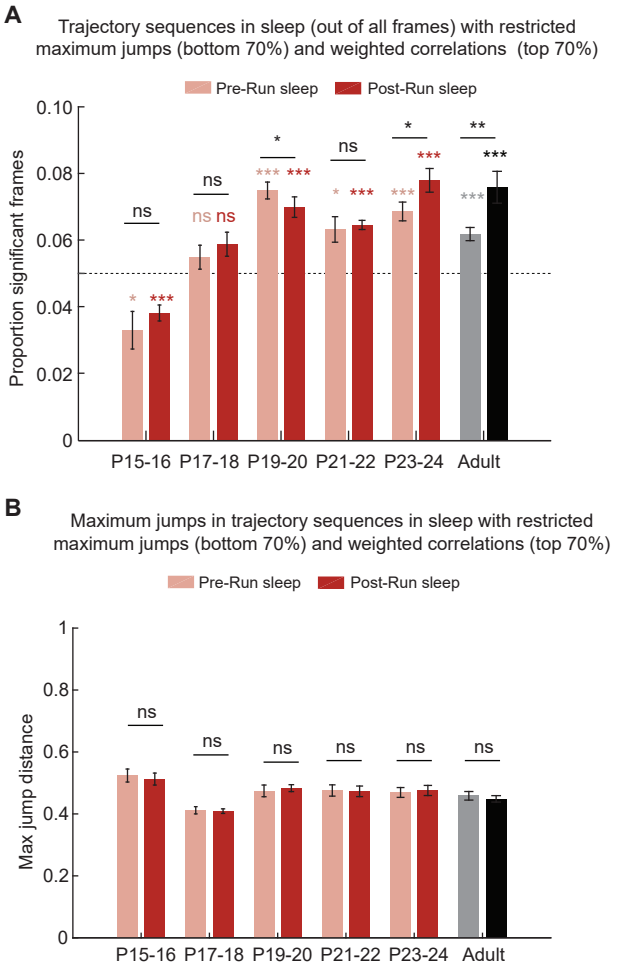

Fig S15. Development of trajectory sequences assessed using more stringent criteria for maximum jump distance and weighted correlation. (**A**) Proportion of significant trajectory sequences calculated by applying two additional criteria for significance in addition to the time-bin shuffle (as a proportion of all detected frames). A significant frame would additionally belong to the top 70th percentile of sleep distribution of weighted correlations and bottom 70th percentile of maximum jump distances. Approximately 50% of all frames across different age groups met these additional stringent criteria. Thus, extended preplay and replay occur significantly above chance levels first at P19-20. (**B**) Maximum jump distance for the significant frames in (**A**). Note a reduction in maximum jumps starting at P17-18 (partial trajectory sequences), compared to P15-16. Data are means ± SEM. ***P<0.005, **P<0.01, *P<0.05, ns=not significant.

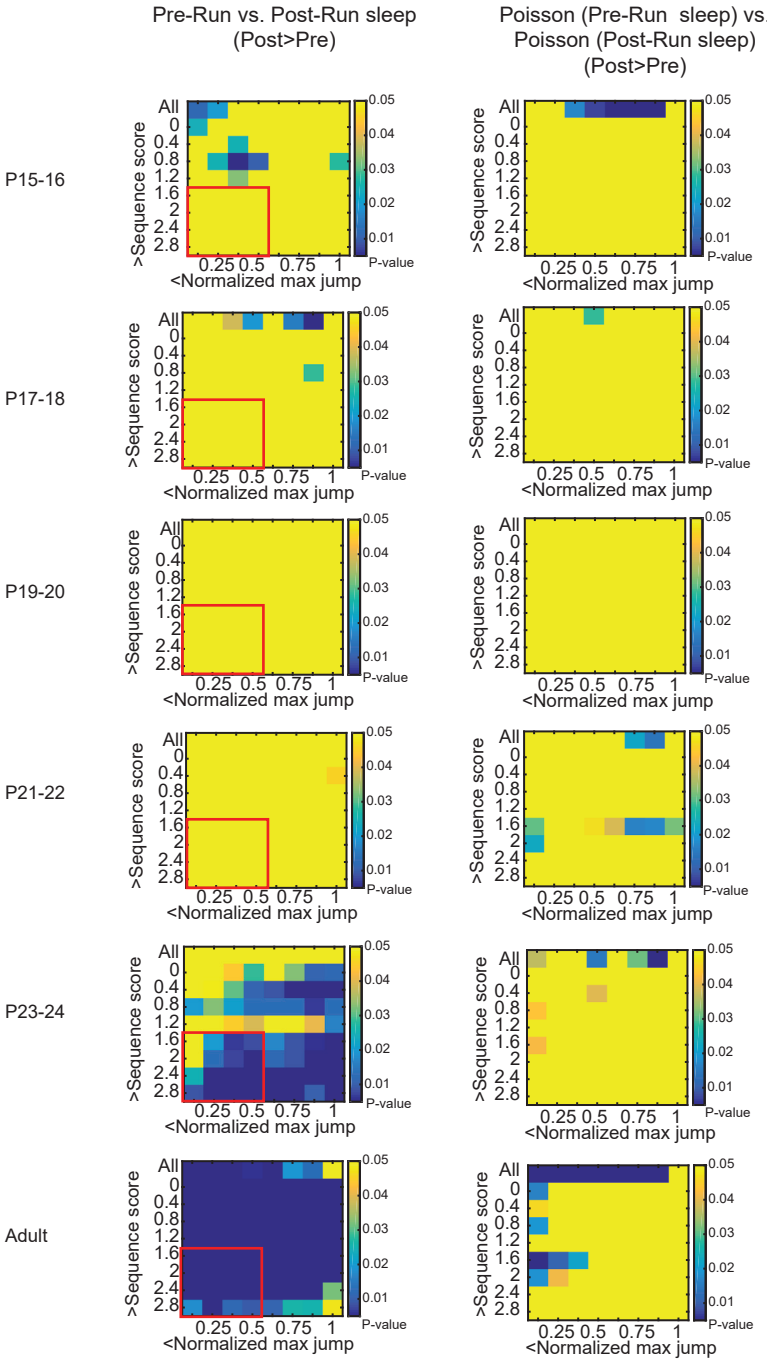

Fig. S16. Two-feature direct comparison of Pre-Run sleep and Post-Run sleep trajectory sequences. Significance matrices for direct comparisons between the proportion of frames passing more rigorous thresholds of sequence scores and normalized maximum jump distances. This comparison reveals that trajectory sequences in Post-Run sleep first become stronger than Pre-Run sleep first at P23-24 (left panels), when they appear adult-like. A similar comparison between sleep firing-rate matched Poisson-distribution datasets for Pre-Run sleep and Post-Run sleep did not reveal a difference. Note the normalized max jump is used to control for the effect of frame length on maximum jump (see Fig. S14). Red squares indicate area of significance with low normalized jumps.

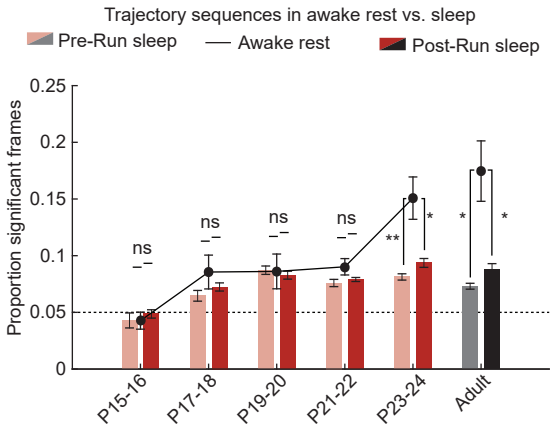

Fig. S17. Comparison of the developmental profile of trajectory sequences during sleep in the sleep box and awake rest on the track. Proportion of Pre-Run sleep, Awake rest (de novo Run) and Post-Run sleep trajectory sequences across development. Note awake replay first increases above Pre-Run sleep (preplay) at P23-24 (paired t-tests). Data are means ± SEM. **P<0.01, *P<0.05, ns=not significant.

Day 1

Age	# of neurons	# of frames	# of Run sessions
P15	60	1209/1501	2
P15	42	1198/1648	2
P15	67	1214/1737	2
P15	30	518/987	1
P16	55	984/1072	1
P17	57	826/629	2
P17	41	669/856	1
P18	35	755/1003	1
P19	36	441/377	2
P19	37	827/1162	2
P20	58	1639/1351	2
P20	28	435/689	2
P21	44	921/1057	2
P22	42	859/742	2
P22	55	1357/1945	1
P22	41	1494/1364	2
P23	65	1619/1458	2
P24	44	1025/1163	2
P24	61	1653/1638	2
Adult	56	4887/1136	2
Adult	50	2937/2083	2
Adult	79	6753/2430	2

Table S1. Details of neuronal recordings across ages. Table contains details of Day 1 of the experiment: animal age, number of neurons simultaneously recorded, number of detected frames in Pre-Run sleep/Post-Run sleep, and number of Run sessions.

References and Notes

1. W. B. Scoville, B. Milner, Loss of recent memory after bilateral hippocampal lesions. *J. Neurol. Neurosurg. Psychiatry* **20**, 11–21 (1957). doi:10.1136/jnnp.20.1.11 Medline

2. L. R. Squire, Memory and the hippocampus: A synthesis from findings with rats, monkeys, and humans. *Psychol. Rev.* **99**, 195–231 (1992). doi:10.1037/0033-295X.99.2.195 Medline

3. H. Eichenbaum, N. J. Cohen, Can we reconcile the declarative memory and spatial navigation views on hippocampal function? *Neuron* **83**, 764–770 (2014). doi:10.1016/j.neuron.2014.07.032 Medline

4. G. Dragoi, S. Tonegawa, Preplay of future place cell sequences by hippocampal cellular assemblies. *Nature* **469**, 397–401 (2011). doi:10.1038/nature09633 Medline

5. A. K. Lee, M. A. Wilson, Memory of sequential experience in the hippocampus during slow wave sleep. *Neuron* **36**, 1183–1194 (2002). doi:10.1016/S0896-6273(02)01096-6 Medline

6. A. Travaglia, R. Bisaz, E. S. Sweet, R. D. Blitzer, C. M. Alberini, Infantile amnesia reflects a developmental critical period for hippocampal learning. *Nat. Neurosci.* **19**, 1225–1233 (2016). doi:10.1038/nn.4348 Medline

7. J. K. Lee, C. Wendelken, S. A. Bunge, S. Ghetti, A Time and Place for Everything: Developmental Differences in the Building Blocks of Episodic Memory. *Child Dev.* **87**, 194–210 (2016). doi:10.1111/cdev.12447 Medline

8. T. J. Wills, F. Cacucci, N. Burgess, J. O'Keefe, Development of the hippocampal cognitive map in preweanling rats. *Science* **328**, 1573–1576 (2010). doi:10.1126/science.1188224 Medline

9. R. F. Langston, J. A. Ainge, J. J. Couey, C. B. Canto, T. L. Bjerknes, M. P. Witter, E. I. Moser, M.-B. Moser, Development of the spatial representation system in the rat. *Science* **328**, 1576–1580 (2010). doi:10.1126/science.1188210 Medline

10. S. Le Vay, T. N. Wiesel, D. H. Hubel, The development of ocular dominance columns in normal and visually deprived monkeys. *J. Comp. Neurol.* **191**, 1–51 (1980). doi:10.1002/cne.901910102 Medline

11. B. L. Benedetti, Y. Takashima, J. A. Wen, J. Urban-Ciecko, A. L. Barth, Differential wiring of layer 2/3 neurons drives sparse and reliable firing during neocortical development. *Cereb. Cortex* **23**, 2690–2699 (2013). doi:10.1093/cercor/bhs257 Medline

12. A. Maffei, G. Turrigiano, The age of plasticity: Developmental regulation of synaptic plasticity in neocortical microcircuits. *Prog. Brain Res.* **169**, 211–223 (2008). doi:10.1016/S0079-6123(07)00012-X Medline

13. J. O'Keefe, L. Nadel, *The Hippocampus as a Cognitive Map*. (Oxford University Press, Oxford, 1978).

14. G. Dragoi, G. Buzsáki, Temporal encoding of place sequences by hippocampal cell assemblies. *Neuron* **50**, 145–157 (2006). doi:10.1016/j.neuron.2006.02.023 Medline

15. G. Dragoi, S. Tonegawa, Distinct preplay of multiple novel spatial experiences in the rat. *Proc. Natl. Acad. Sci. U.S.A.* **110**, 9100–9105 (2013). doi:10.1073/pnas.1306031110 Medline

16. F. Donato, R. I. Jacobsen, M. B. Moser, E. I. Moser, Stellate cells drive maturation of the entorhinal-hippocampal circuit. *Science* **355**, eaai8178 (2017). doi:10.1126/science.aai8178 Medline

17. L. Muessig, J. Hauser, T. J. Wills, F. Cacucci, A Developmental Switch in Place Cell Accuracy Coincides with Grid Cell Maturation. *Neuron* **86**, 1167–1173 (2015). doi:10.1016/j.neuron.2015.05.011 Medline

18. W. E. Skaggs, B. L. McNaughton, M. A. Wilson, C. A. Barnes, Theta phase precession in hippocampal neuronal populations and the compression of temporal sequences. *Hippocampus* **6**, 149–172 (1996). doi:10.1002/(SICI)1098-1063(1996)6:2<149:AID-HIPO6>3.0.CO;2-K Medline

19. S. J. Middleton, T. J. McHugh, Silencing CA3 disrupts temporal coding in the CA1 ensemble. *Nat. Neurosci.* **19**, 945–951 (2016). doi:10.1038/nn.4311 Medline

20. M. I. Schlesiger, C. C. Cannova, B. L. Boublil, J. B. Hales, E. A. Mankin, M. P. Brandon, J. K. Leutgeb, C. Leibold, S. Leutgeb, The medial entorhinal cortex is necessary for temporal organization of hippocampal neuronal activity. *Nat. Neurosci.* **18**, 1123–1132 (2015). doi:10.1038/nn.4056 Medline

21. G. Dragoi, S. Tonegawa, Development of schemas revealed by prior experience and NMDA receptor knock-out. *eLife* **2**, e01326 (2013). doi:10.7554/eLife.01326 Medline

22. Y. Wang, S. Romani, B. Lustig, A. Leonardo, E. Pastalkova, Theta sequences are essential for internally generated hippocampal firing fields. *Nat. Neurosci.* **18**, 282–288 (2015). doi:10.1038/nn.3904 Medline

23. E. Pastalkova, V. Itskov, A. Amarasingham, G. Buzsáki, Internally generated cell assembly sequences in the rat hippocampus. *Science* **321**, 1322–1327 (2008). doi:10.1126/science.1159775 Medline

24. D. J. Foster, M. A. Wilson, Reverse replay of behavioural sequences in hippocampal place cells during the awake state. *Nature* **440**, 680–683 (2006). doi:10.1038/nature04587 Medline

25. T. J. Davidson, F. Kloosterman, M. A. Wilson, Hippocampal replay of extended experience. *Neuron* **63**, 497–507 (2009). doi:10.1016/j.neuron.2009.07.027 Medline

26. A. V. Egorov, B. N. Hamam, E. Fransén, M. E. Hasselmo, A. A. Alonso, Graded persistent activity in entorhinal cortex neurons. *Nature* **420**, 173–178 (2002). doi:10.1038/nature01171 Medline

27. G. Dragoi, S. Tonegawa, Selection of preconfigured cell assemblies for representation of novel spatial experiences. *Philos. Trans. R. Soc. Lond. B Biol. Sci.* **369**, 20120522 (2013). doi:10.1098/rstb.2012.0522 Medline

28. A. D. Grosmark, G. Buzsáki, Diversity in neural firing dynamics supports both rigid and learned hippocampal sequences. *Science* **351**, 1440–1443 (2016). doi:10.1126/science.aad1935 Medline

29. I. Kant, *Critique of Pure Reason*. (Cambridge University Press, Cambridge, UK, 1781).

30. J. Yamamoto, S. Tonegawa, Direct Medial Entorhinal Cortex Input to Hippocampal CA1 Is Crucial for Extended Quiet Awake Replay. *Neuron* **96**, 217–227.e4 (2017). doi:10.1016/j.neuron.2017.09.017 Medline

31. N. Schmitzer-Torbert, J. Jackson, D. Henze, K. Harris, A. D. Redish, Quantitative measures of cluster quality for use in extracellular recordings. *Neuroscience* **131**, 1–11 (2005). doi:10.1016/j.neuroscience.2004.09.066 Medline

32. K. Zhang, I. Ginzburg, B. L. McNaughton, T. J. Sejnowski, Interpreting neuronal population activity by reconstruction: Unified framework with application to hippocampal place cells. *J. Neurophysiol.* **79**, 1017–1044 (1998). doi:10.1152/jn.1998.79.2.1017 Medline

33. D. Silva, T. Feng, D. J. Foster, Trajectory events across hippocampal place cells require previous experience. *Nat. Neurosci.* **18**, 1772–1779 (2015). doi:10.1038/nn.4151 Medline